# Inherited structure as a control on late Paleozoic and Mesozoic exhumation of the Tarbagatai Mountains, southeastern Kazakhstan

Jack Gillespie[1,2], Stijn Glorie[1], Gilby Jepson[1,3], Fedor Zhimulev[4], Dmitriy Gurevich[5], Martin Danišík[6], and Alan S. Collins[1]

[1]Department of Earth Sciences, School of Physical Science, The University of Adelaide, SA 5005, Australia
[2]The Institute for Geoscience Research (TIGeR), School of Earth and Planetary Sciences, Curtin University, Perth, Australia
[3]Department of Geoscience, University of Arizona, Tucson, Arizona, USA
[4]Sobolev Institute of Geology and Mineralogy, Siberian Branch Russian Academy of Sciences, Novosibirsk 630090, Koptuga Ave 3, Russia
[5]SRK Exploration, Moscow, Russia
[6]John de Laeter Centre, TIGeR, School of Earth and Planetary Sciences, Curtin University, Perth, Australia

January 28, 2021

## Contents



# 1 Introduction

The supporting information presented here is divided into three sections, consisting of the supporting descriptive text, summary data and plots for the apatite fission track analysis, apatite U-Pb dating, and the thermal history modelling. For individual grain/spot analytical data and tables of confined track lengths, see the separate attached supplementary data tables.

# List of Figures



# List of Tables



**Additional supporting information - uploaded separately**: Large Tables S3, S4, S5

# 2 Apatite fission track supplementary information

## 2.1 Data description

### 2.1.1 Balkhash-Yili

Samples TA-01, TA-07, and TA-27 were sampled from the area immediately to the south-east of the Chingiz-Tabagatai Fault, from the Balkhash-Yili arc. Sample TA-01 produced a central age of 204.5 ± 8.6 Ma, with a dispersion of 12% (n=37) and a P($\chi^2$) value of 0.14. Confined track length measurement yielded a mean track length (MTL) of 13.5 ± 1.1 µm (n=100). Sample TA-07 produced a central age of 213.4 ± 12.1 Ma, with a dispersion of 6% (n=34) and a P($\chi^2$) value of 0.29. Confined track length measurement yielded a MTL of 13.1 ± 1.3 µm (n=101). Sample TA-27 produced a central age of 186.6 ± 7.4 Ma, with a dispersion of 0% (n=17) and a P($\chi^2$) value of 0.65.

### 2.1.2 Southern Boshchekul-Chingiz

Samples taken from the Boshchekul-Chingiz arc can be divided into two categories based on their geographical location and proximity to NW-SE trending faults. Samples TA-02, TA-04, TA-05, TA-06, TA-10, TA-11, and TA-16 are in the southern section of the sampling area and are generally proximal to NW-SE striking faults. Sample TA-02 produced a central age of 258.7 ± 31.3 Ma, with a dispersion of 29% (n=20) and a P($\chi^2$) value of 0.13. Sample TA-04 produced a central age of 212.7 ± 20.6 Ma, with a dispersion of 11% (n=25) and a P($\chi^2$) value of 0.40. Sample TA-05 produced a central age of 156.8 ± 26.5 Ma, with a dispersion of 0% (n=4) and a P($\chi^2$) value of 0.40. Sample TA-06 produced a central age of 132.5 ± 6.0 Ma, with a dispersion of 7% (n=38) and a P($\chi^2$) value of 0.65. Confined track length measurement produced a MTL of 13.1 ± 1.1 µm (n=119). Sample TA-10 produced a central age of 168.3 ± 5.7 Ma, with a dispersion of 9% (n=36) and a P($\chi^2$) value of 0.10. Confined track length measurement produced a MTL of 13.0 ± 1.4 µm (n=100). Sample TA-11 produced a central age of 148.4 ± 8.3 Ma, with a dispersion of 12% (n=27) and a P($\chi^2$) value of 0.16. Confined track length measurement produced a MTL of 12.1 ± 1.5 µm (n=42). Sample TA-16 produced a central age of 150.0 ± 10.3 Ma, with a dispersion of 21% (n=32) and a P($\chi^2$) value of 0.02. Confined track length measurement produced a MTL of 13.2 ± 1.4 µm (n=65).

### 2.1.3 Northern Boshchekul-Chingiz

Samples TA-14, TA-15, TA-17, TA-18, TA-19, and TA-26 lie in the north of the sampled section of the Boshchekul-Chingiz arc. Sample TA-14 produced a central age of 209.7 ± 9.2 Ma, with a dispersion of 0% (n=31) and a P($\chi^2$) value of 0.84. Confined track length measurement produced a MTL of 13.0 ± 1.5 µm (n=106). Sample TA-15 produced a central age of 197.3 ± 18.8 Ma, with a dispersion of 35% (n=21) and a P($\chi^2$) value of 0.00. Confined track length measurement produced a MTL of 12.1 ± 1.7 µm (n=32). Sample TA-17 produced a central age of 192.3 ± 9.7 Ma, with a dispersion of 19% (n=34) and a P($\chi^2$) value of 0.00. Confined track length measurement produced a MTL of 12.3 ± 1.9 µm (n=116). Sample TA-18 produced a central age of 301.1 ± 17.3 Ma, with a dispersion of 21% (n=26) and a P($\chi^2$) value of 0.00. Confined track length measurement produced a MTL of 12.7 ± 1.4 µm (n=54). Sample TA-19 produced a central age of 184.5 ± 13.5 Ma, with a dispersion of 30% (n=30) and a P($\chi^2$) value of 0.00. Confined track length measurement produced a MTL of 12.5 ± 1.6 µm (n=98). Sample TA-26 produced a central age of 214.1 ± 7.4 Ma, with a dispersion of 11% (n=38) and a P($\chi^2$) value of 0.07. Confined track length measurement produced a MTL of 13.2 ± 1.2 µm (n=102).

### 2.1.4 Zharma-Saur

Samples TA-20, TA-22, and TA-23 were taken from the Zharma-Saur arc, to the north-east of the Boshchekul-Chingiz arc. Sample TA-20 produced a central age of 258.4 ± 7.3 Ma, with a dispersion of 0% (n=40) and

a P($\chi^2$) value of 0.90. Confined track length measurement yielded a MTL of 13.6 ± 1.1 µm (n=45). Sample TA-22 produced a central age of 254.3 ± 10.6 Ma, with a dispersion of 10% (n=39) and a P($\chi^2$) value of 0.21. Confined track length measurement yielded a MTL of 13.8 ± 0.9 µm (n=71). Sample TA-23 produced a central age of 251.4 ± 13.0 Ma, with a dispersion of 23% (n=36) and a P($\chi^2$) value of 0.00. Confined track length measurement yielded a MTL of 13.3 ± 1.2 µm (n=91).

## 2.2 Figures

Figure S1: Apatite fission track radial plots.

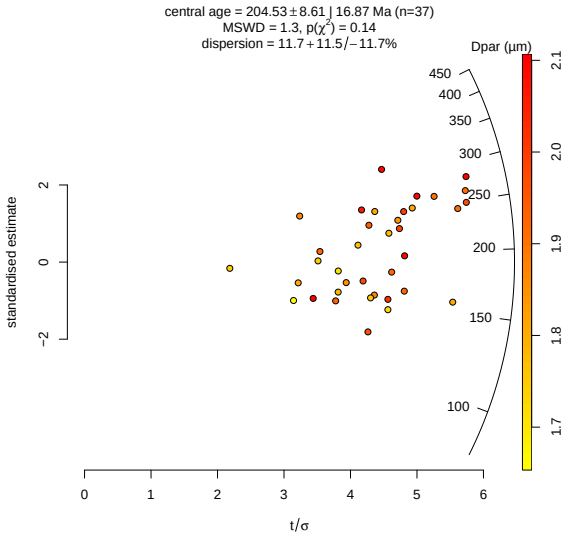


(a) Radial plot for TA01

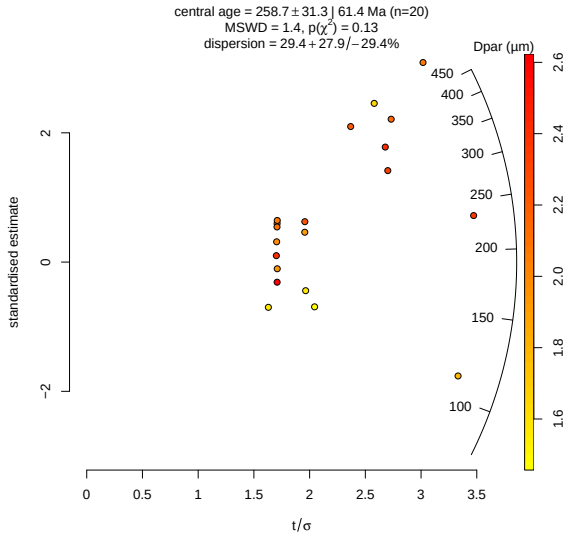


(b) Radial plot for TA02

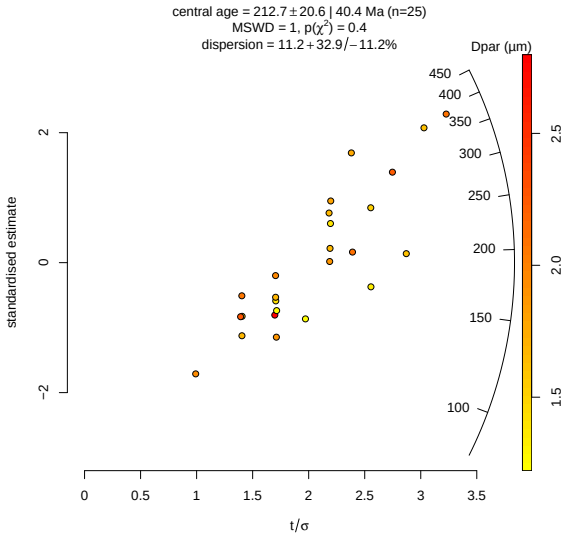


(c) Radial plot for TA04

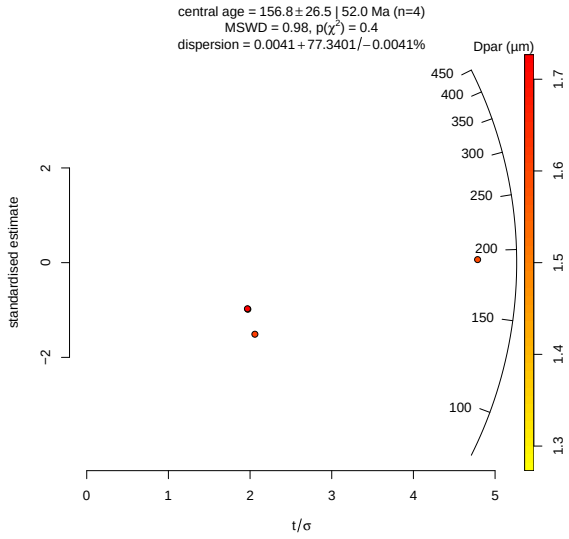


(d) Radial plot for TA05

Figure S2: Apatite fission track radial plots

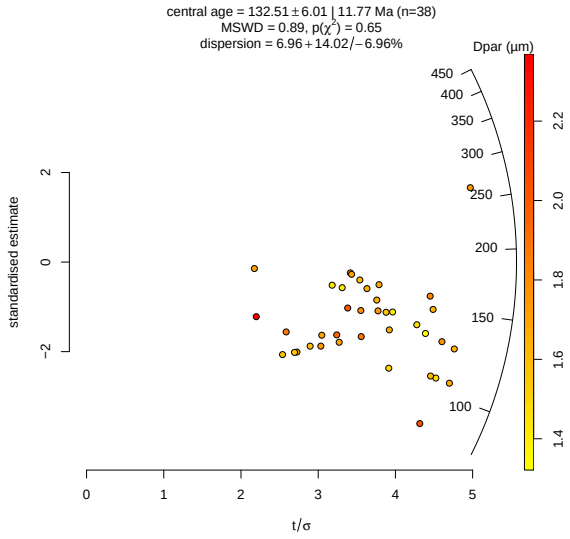


(a) Radial plot for TA06

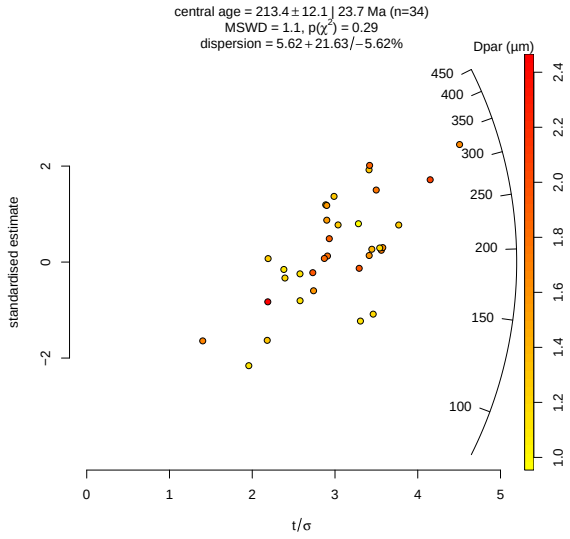


(b) Radial plot for TA07

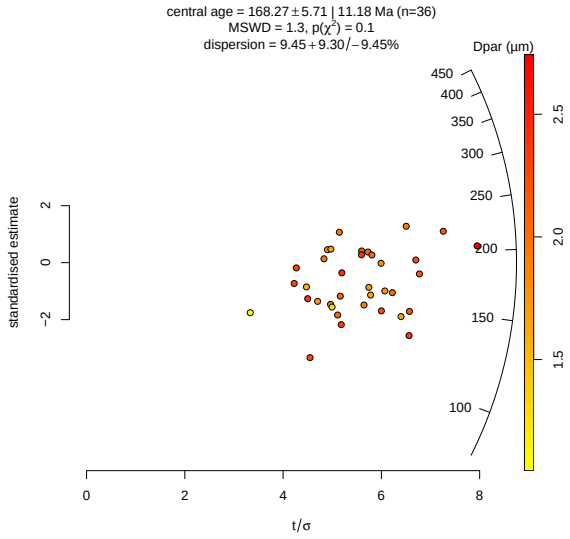


(c) Radial plot for TA10

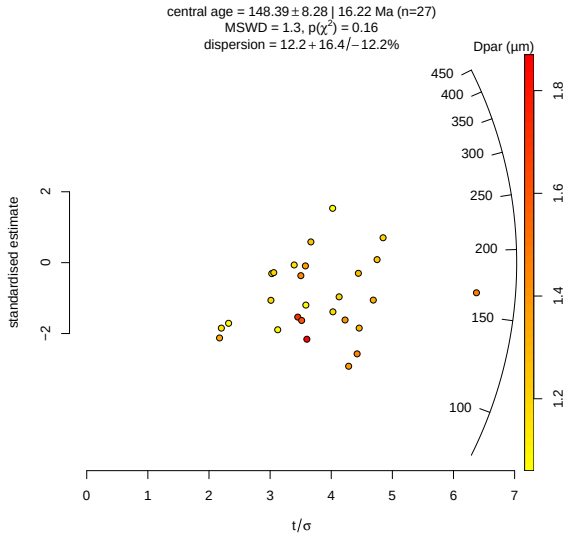


(d) Radial plot for TA11

Figure S3: Apatite fission track radial plots

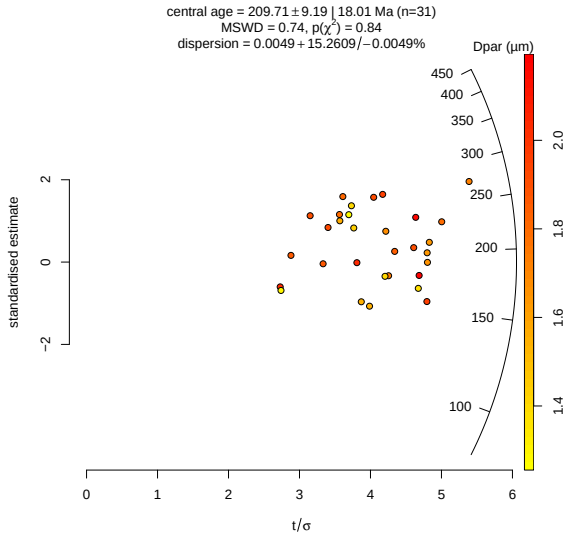


(a) Radial plot for TA14

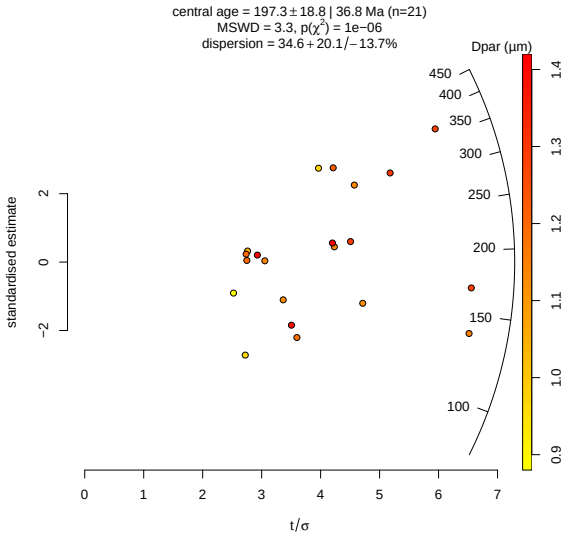


(b) Radial plot for TA15

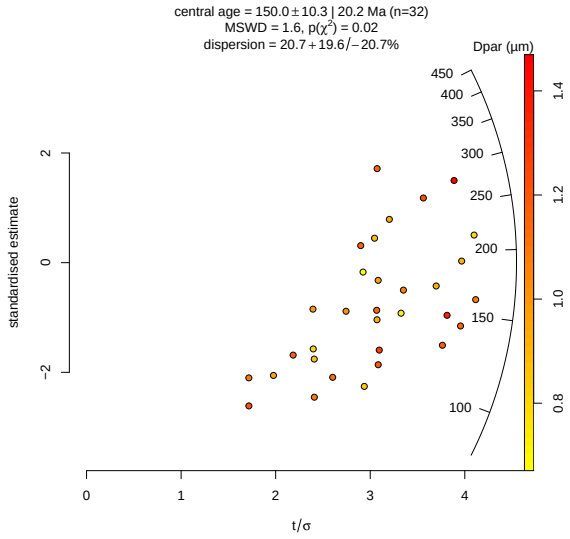


(c) Radial plot for TA16

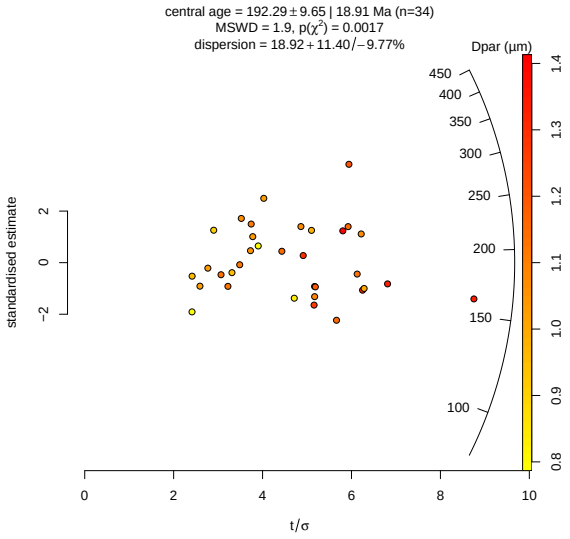


(d) Radial plot for TA17

Figure S4: Apatite fission track radial plots

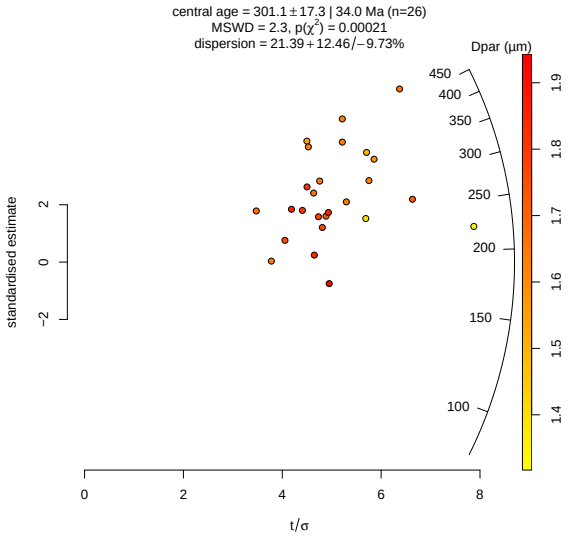


(a) Radial plot for TA18

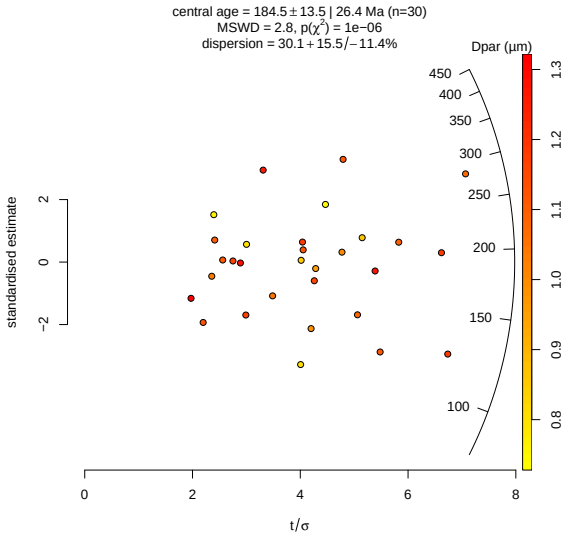


(b) Radial plot for TA19

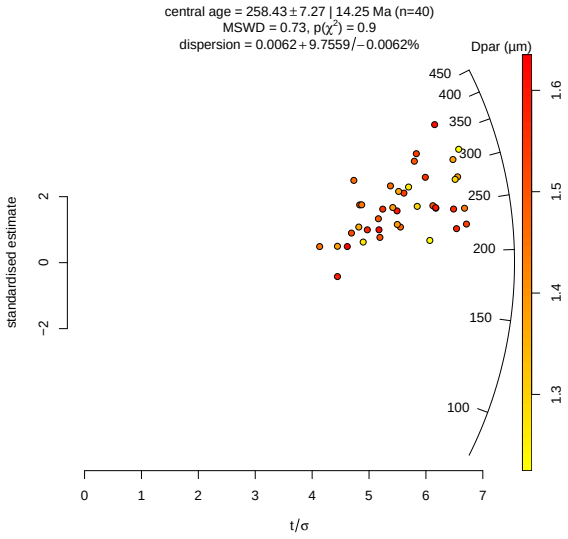


(c) Radial plot for TA20

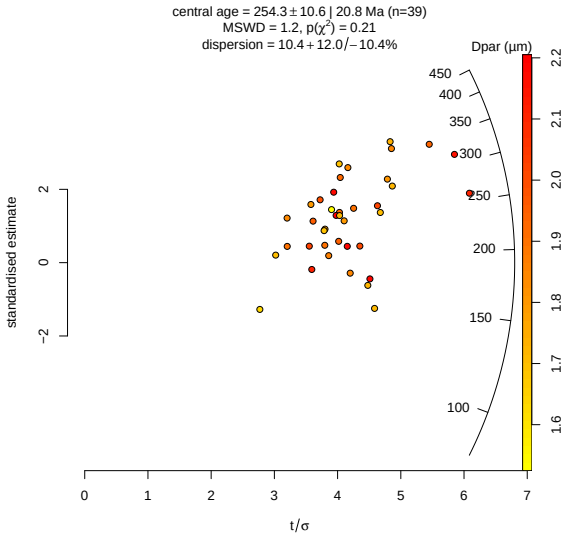


(d) Radial plot for TA22

Figure S5: Apatite fission track radial plots

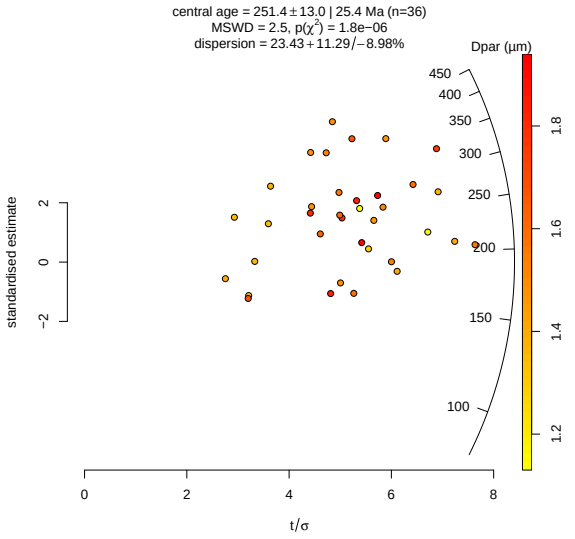


(a) Radial plot for TA23

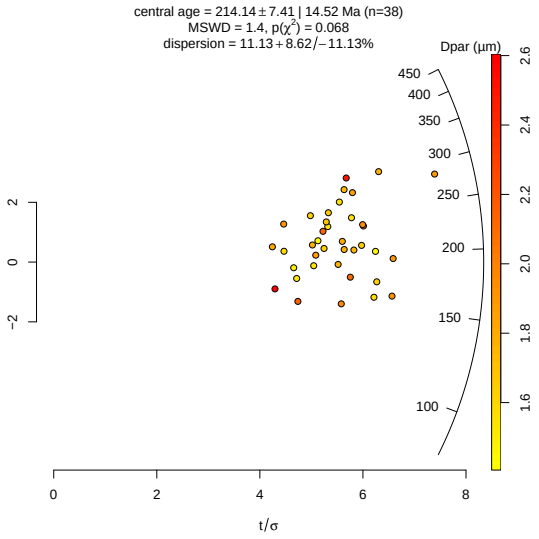


(b) Radial plot for TA26

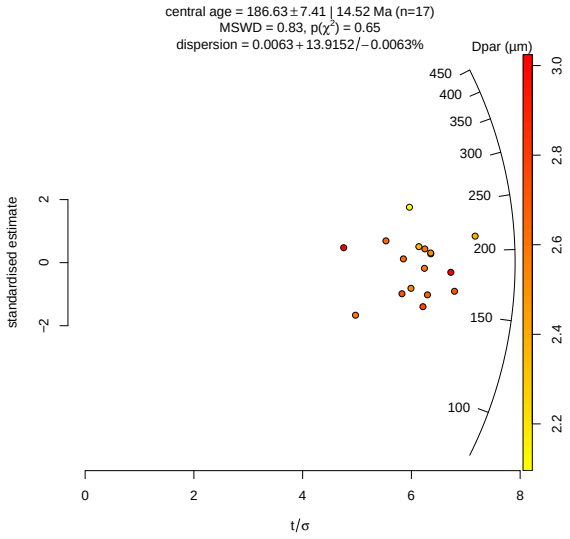


(c) Radial plot for TA27

Figure S6: Apatite confined track length histograms

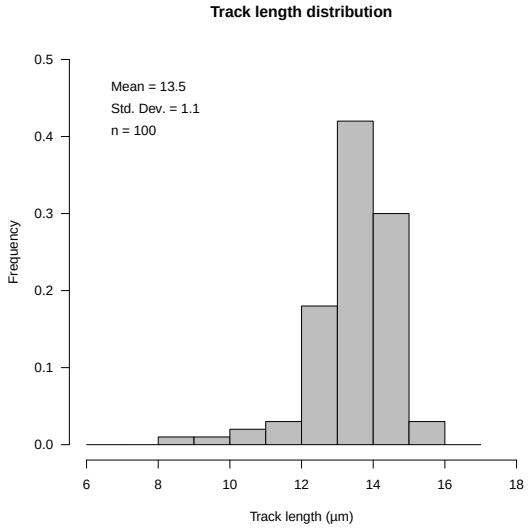


(a) Confined track length histogram for TA01

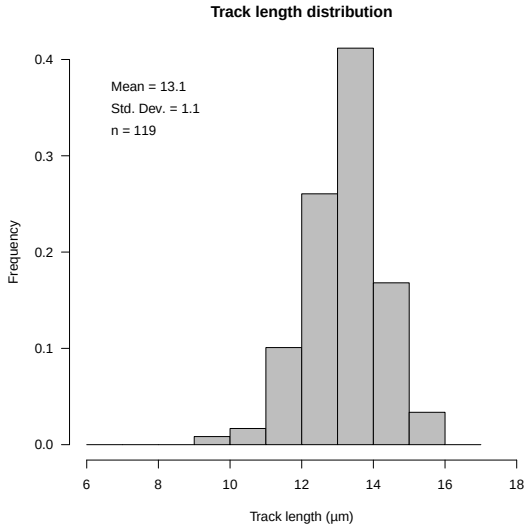


(b) Confined track length histogram for TA06

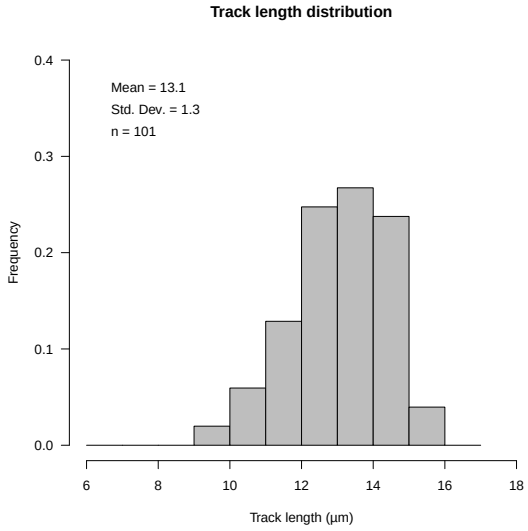


(c) Confined track length histogram for TA07

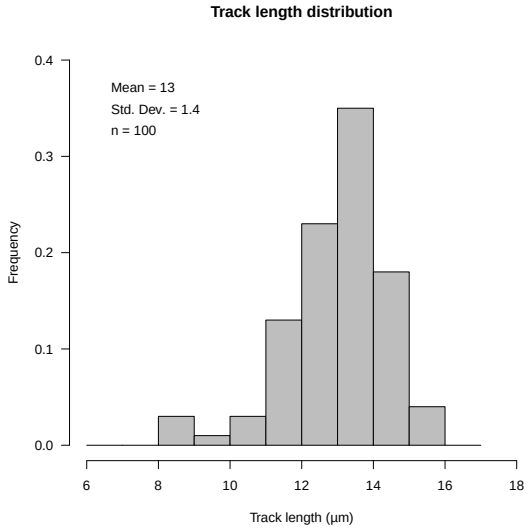


(d) Confined track length histogram for TA10

Figure S7: Apatite confined track length histograms

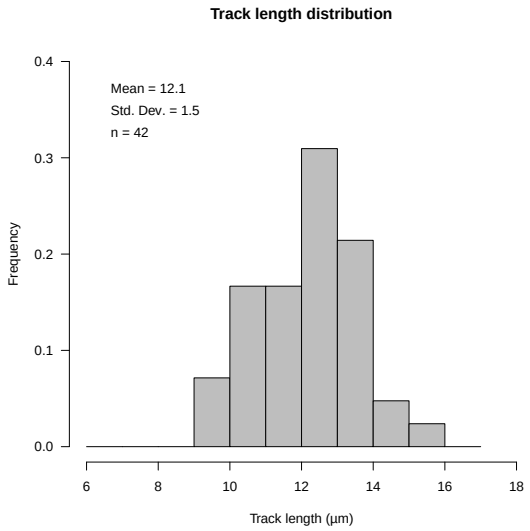


(a) Confined track length histogram for TA11

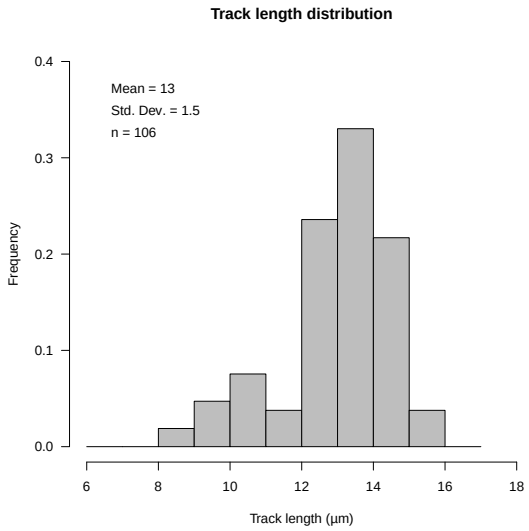


(b) Confined track length histogram for TA14

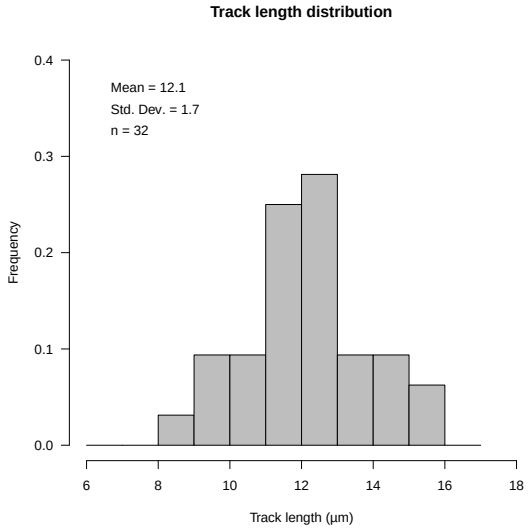


(c) Confined track length histogram for TA15

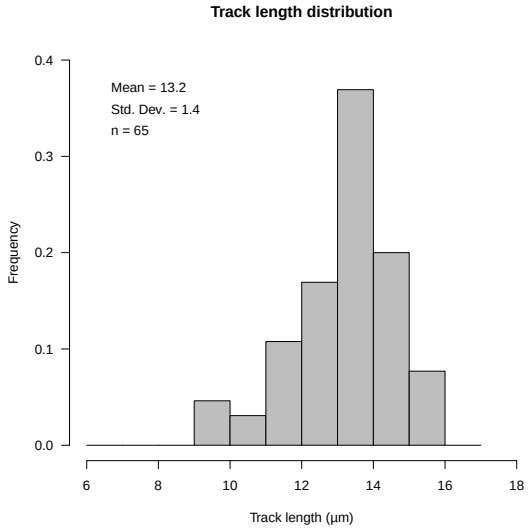


(d) Confined track length histogram for TA16

Figure S8: Apatite confined track length histograms

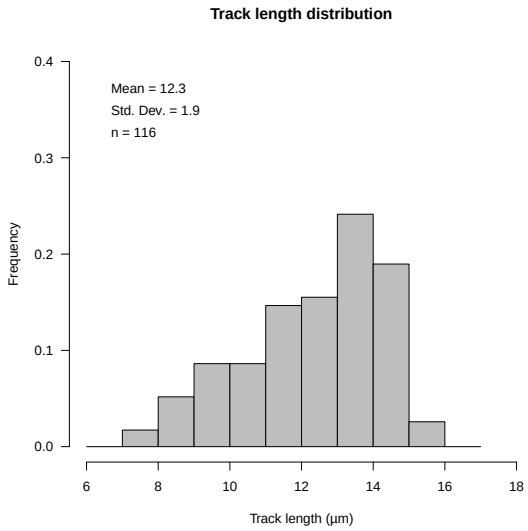


(a) Confined track length histogram for TA17

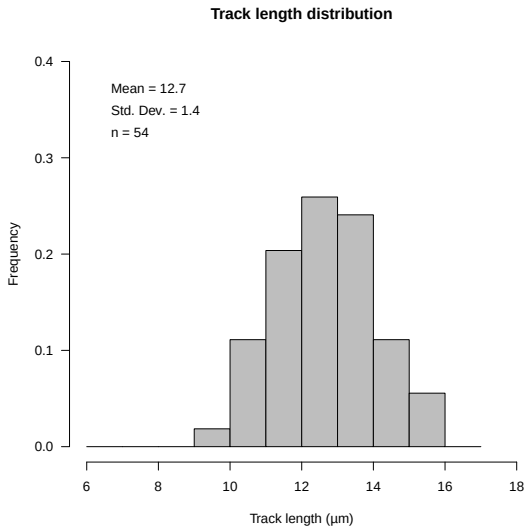


(b) Confined track length histogram for TA18

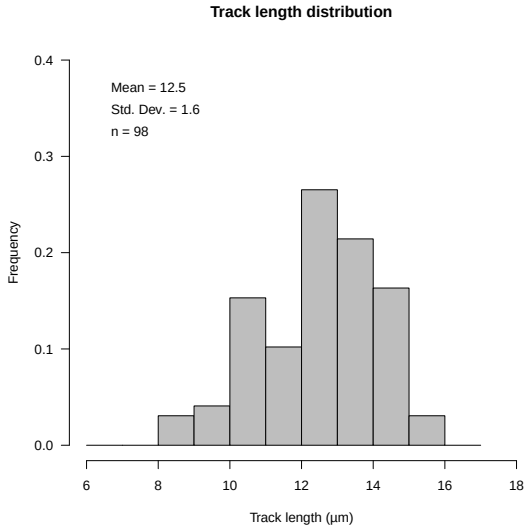


(c) Confined track length histogram for TA19

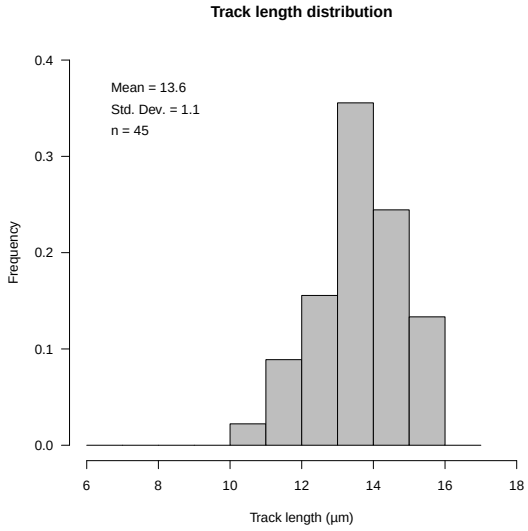


(d) Confined track length histogram for TA20

Figure S9: Apatite confined track length histograms

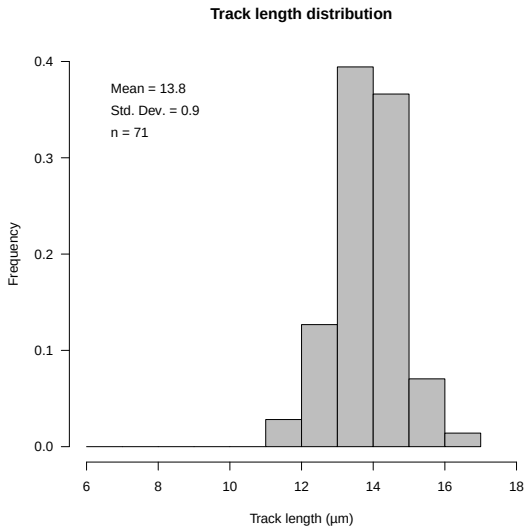


(a) Confined track length histogram for TA22

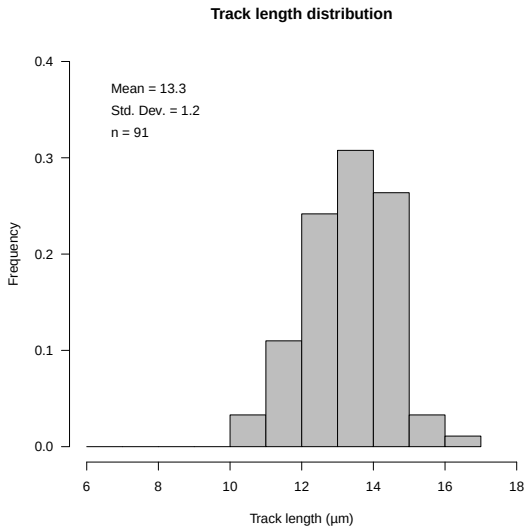


(b) Confined track length histogram for TA23

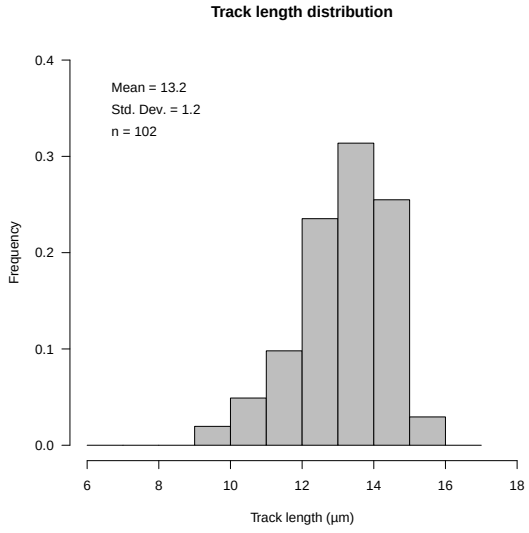


(c) Confined track length histogram for TA26

# 3 Apatite U–Pb data

Table S1: Apatite U-Pb data summary table

| Sample | U-Pb age (Ma) | 0.95 CI (Ma) | $(^{207}Pb/^{206}Pb)_o$ | 0.95 CI | MSWD | $P(\chi^2)$ | n |
|---|---|---|---|---|---|---|---|
| TA01 | 349.4 | 19.8 | 0.818 | 0.042 | 0.7 | 0.92 | 39 |
| TA02 | 384.6 | 23.1 | 0.847 | 0.023 | 1.6 | 0.057 | 19 |
| TA06 | 314.6 | 30.9 | 0.856 | 0.04 | 1.1 | 0.36 | 37 |
| TA07 | 313.5 | 15.3 | 0.869 | 0.032 | 1.2 | 0.2 | 40 |
| TA10 | 417.2 | 14.7 | 0.844 | 0.073 | 0.96 | 0.52 | 31 |
| TA11 | 396.6 | 10.9 | 0.891 | 0.031 | 1.1 | 0.37 | 31 |
| TA14 | 298.6 | 21.1 | 0.854 | 0.032 | 1.1 | 0.34 | 33 |
| TA15 | 320.5 | 19.3 | 0.86 | 0.035 | 5.1 | 0 | 18 |
| TA16 | 410.6 | 18.8 | 0.897 | 0.027 | 1 | 0.45 | 36 |
| TA17 | 282.0 | 9.7 | 0.868 | 0.0093 | 1.1 | 0.25 | 40 |
| TA18 | 329.9 | 10.4 | 0.884 | 0.02 | 1.2 | 0.17 | 29 |
| TA19 | 323.4 | 11.5 | 0.886 | 0.011 | 1.1 | 0.31 | 30 |
| TA22 | 326.8 | 20.9 | 0.89 | 0.016 | 1.1 | 0.32 | 40 |
| TA23 | 317.5 | 7.5 | 0.878 | 0.013 | 1.2 | 0.18 | 39 |
| TA26 | 324.7 | 24.1 | 0.882 | 0.033 | 0.8 | 0.8 | 40 |
| TA27 | 309.9 | 20.3 | 0.82 | 0.104 | 0.97 | 0.48 | 17 |
| *Poorly defined* | | | | | | | |
| *TA04* | *241.6* | *97.5* | *0.744* | *0.047* | *3* | *0* | *17* |
| *TA05* | *400.4* | *155.9* | *0.901* | *0.192* | *4* | *0.018* | *4* |
| *TA20* | *353.2* | *72.9* | *0.891* | *0.04* | *1.1* | *0.32* | *40* |

U-Pb age refers to the lower concordia intercept age calculated by IsoplotR (Vermeesch, 2018). 0.95 CI is the 95% confidence interval of the calculated value. $(^{207}Pb/^{206}Pb)_o$ is the upper (y-axis) intercept of the linear regression through apatite U-Pb analyses.

Figure S10: Apatite U-Pb Tera-Wasserburg inverse concordia diagrams. Ellipses are 2σ. Black line is linear regression through apatite U-Pb data. Grey envelope indicates range of 95% confidence interval of linear regression. Dashed ellipses indicate analyses excluded from linear regression.

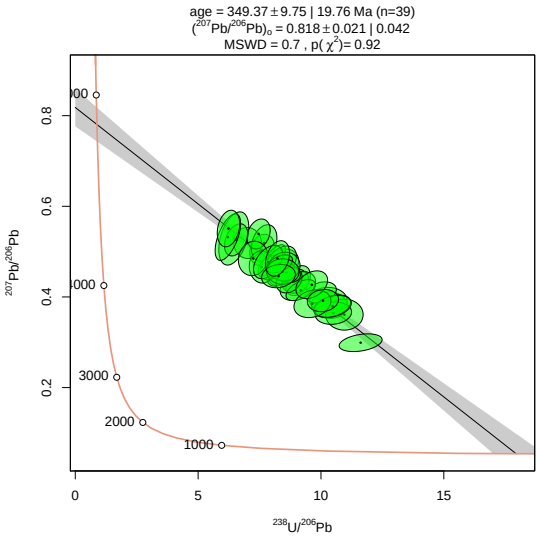


(a) T-W diagram for TA01

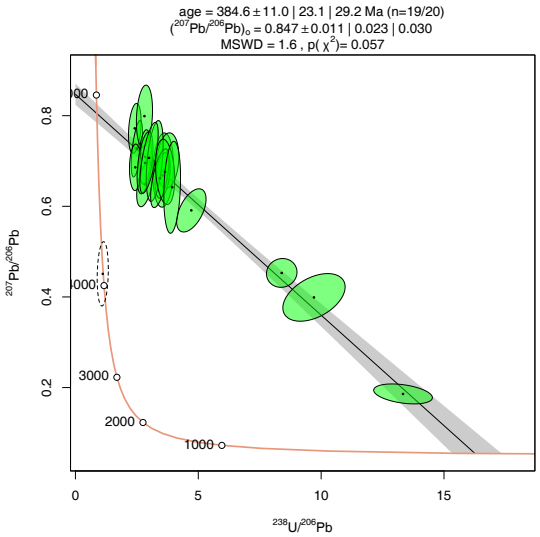


(b) T-W diagram for TA02

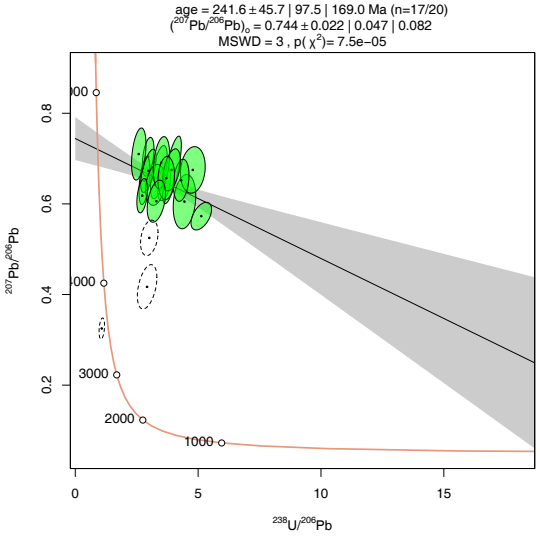


(c) T-W diagram for TA04

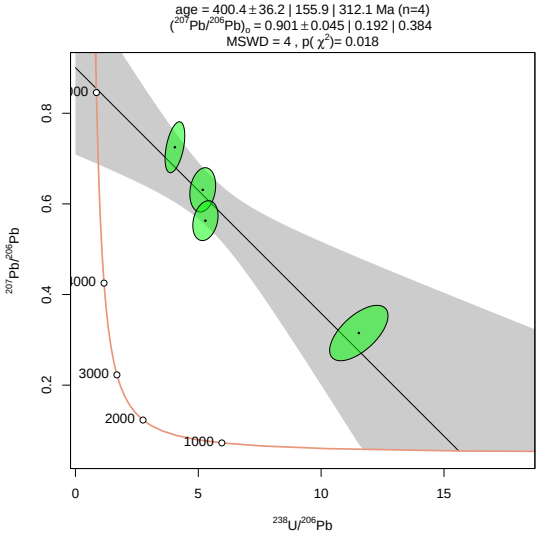


(d) T-W diagram for TA05

Figure S11: Apatite U-Pb Tera-Wasserburg inverse concordia diagrams

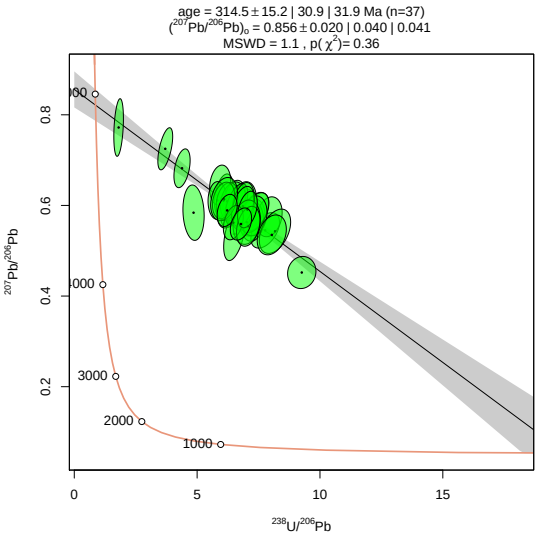


(a) T-W diagram for TA06

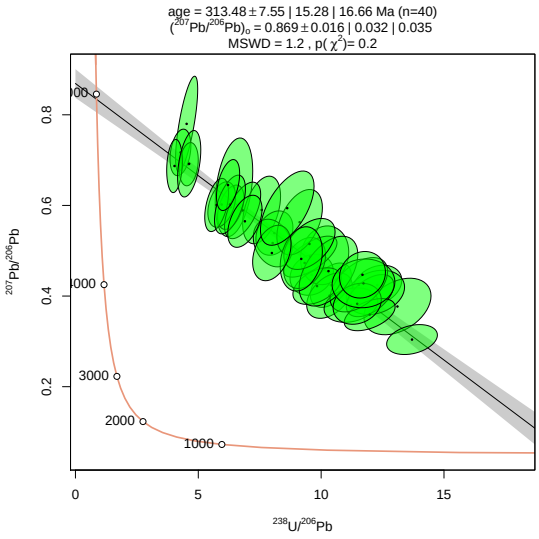


(b) T-W diagram for TA07

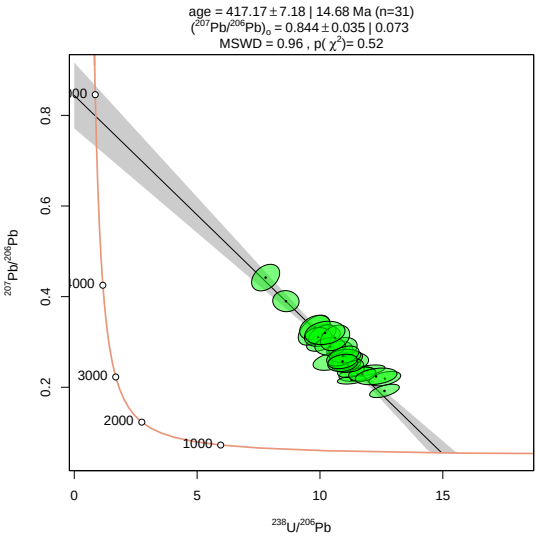


(c) T-W diagram for TA10

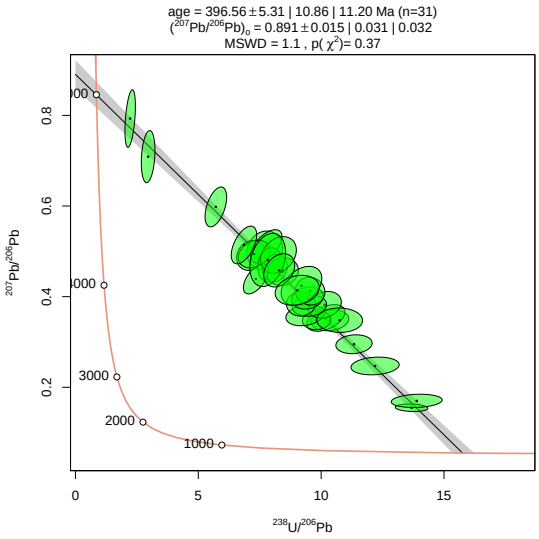


(d) T-W diagram for TA11

Figure S12: Apatite U-Pb Tera-Wasserburg inverse concordia diagrams

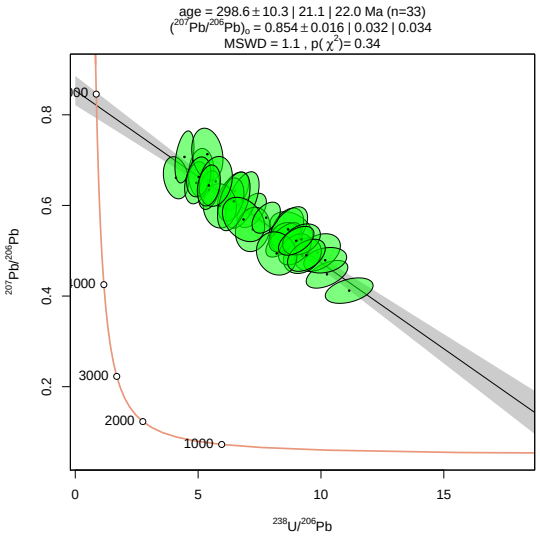


(a) T-W diagram for TA14

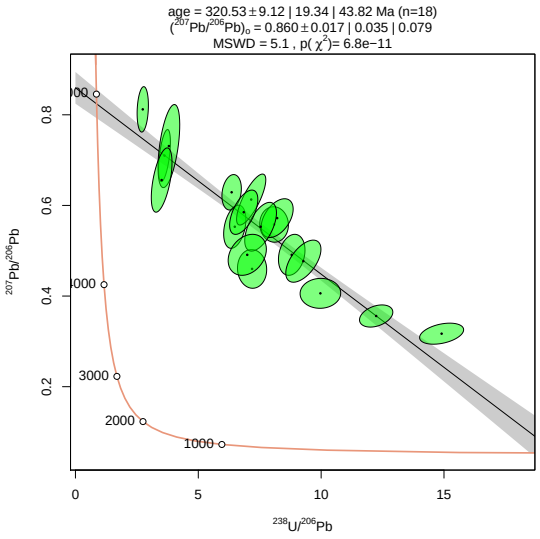


(b) T-W diagram for TA15

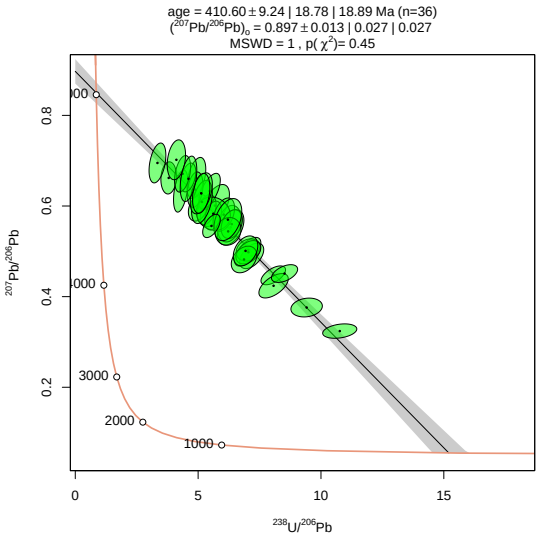


(c) T-W diagram for TA16

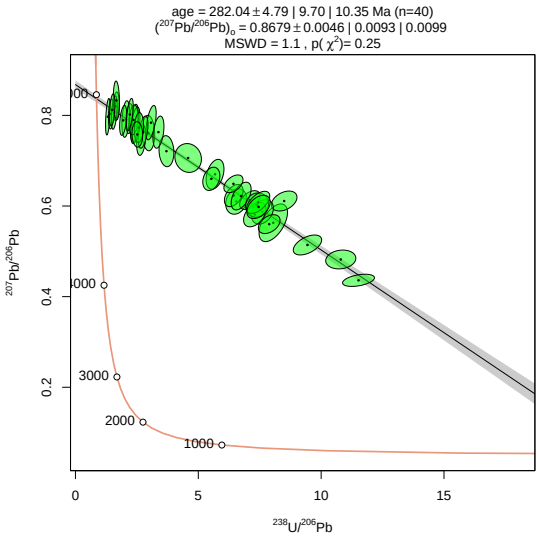


(d) T-W diagram for TA17

Figure S13: Apatite U-Pb Tera-Wasserburg inverse concordia diagrams

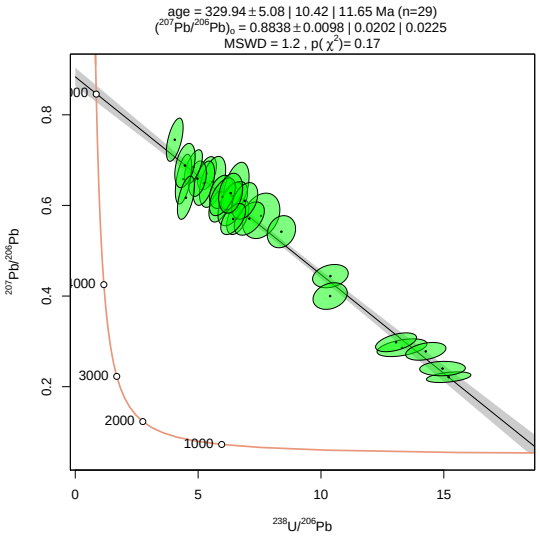


(a) T-W diagram for TA18

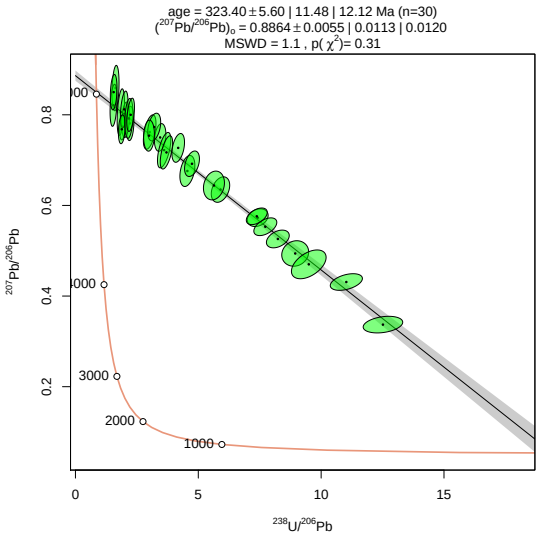


(b) T-W diagram for TA19

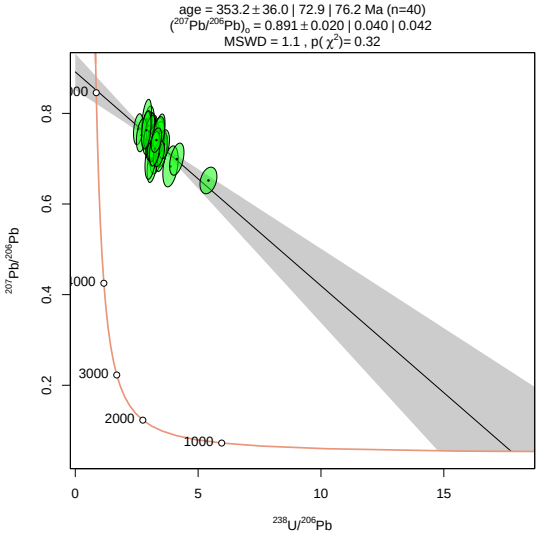


(c) T-W diagram for TA20

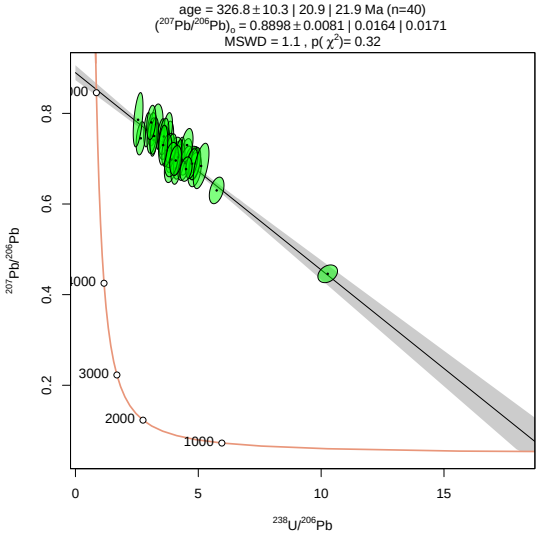


(d) T-W diagram for TA22

Figure S14: Apatite U-Pb Tera-Wasserburg inverse concordia diagrams

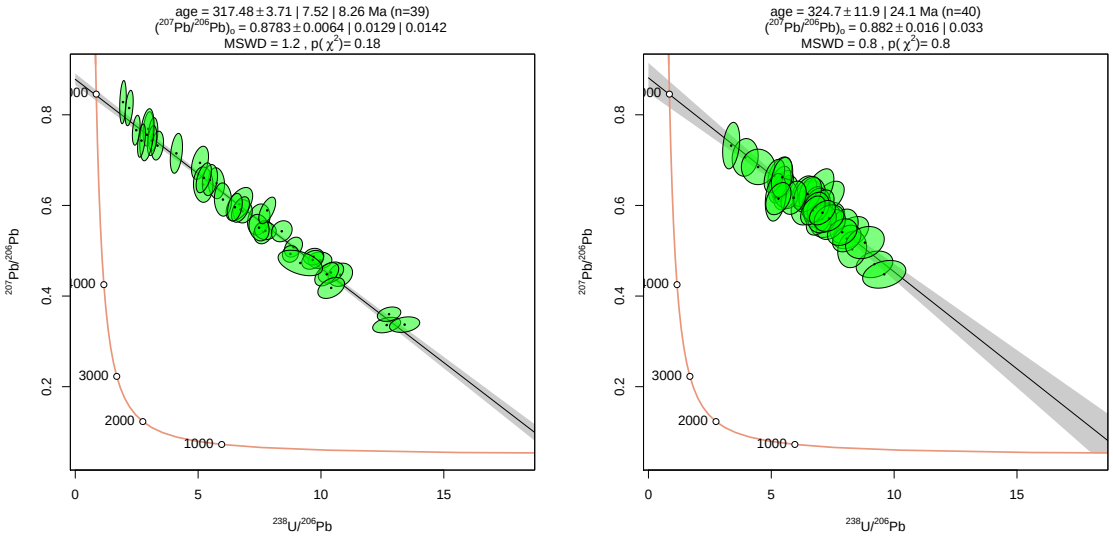


(a) T-W diagram for TA23

(b) T-W diagram for TA26

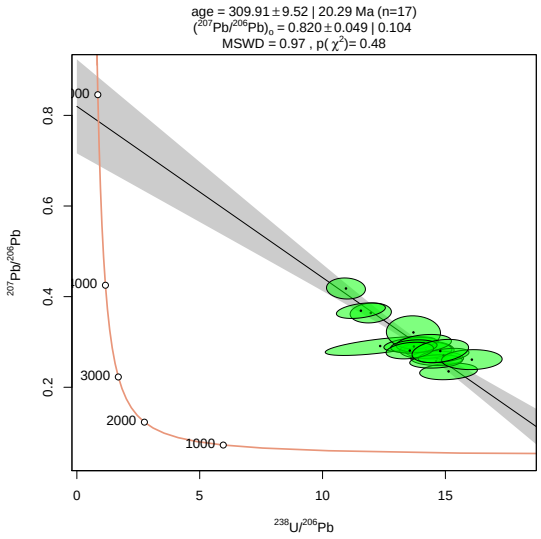


(c) T-W diagram for TA27

# 4 Thermal history modelling

This section contains data and plots that summarize the thermal history modelling carried out as part of this study, including the outputs from the individual thermal history models generated in QTQt showing the observed and predicted values for the inputs.

Table S2: Thermal history modelling inputs, assumptions, and parameters

**1. Thermochronological data**

| **Model input data** | | | Data Source | Published data? |
|---|---|---|---|---|
| Sample Region | AHe | AFT | | |
| *Balkhash-Yili* | | | | |
| TA01 | | x | (1) | Y |
| TA07 | | x | (1) | Y |
| *Boshchekul-Chingiz (S)* | | | | |
| TA06 | x | x | (1) | Y |
| TA10 | x | x | (1) | Y |
| TA11 | | x | (1) | Y |
| TA16 | x | x | (1) | Y |
| *Boshchekul-Chingiz (N)* | | | | |
| TA14 | | x | (1) | Y |
| TA15 | | x | (1) | Y |
| TA17 | | x | (1) | Y |
| TA18 | | x | (1) | Y |
| TA19 | | x | (1) | Y |
| TA26 | | x | (1) | Y |
| *Zharma-Saur* | | | | |
| TA20 | | x | (1) | Y |
| TA22 | | x | (1) | Y |
| TA23 | | x | (1) | Y |

**Data treatment, uncertainties, and other relevant constraints**

*He data*

Treatment: Each individual analysis input separately into QTQt

Dates (Ma): Uncorrected He date input, α-ejection correction applied in QTQt after (Farley et al., 1996)

Uncertainties (Ma): Analytical uncertainties (1σ) input and resampled with MCMC procedure to account for overdispersion of dates due to sources of uncertainty in He dating that are difficult to quantify

r (µm): Mean equivalent spherical radius of each sample

*AFT data*

Initial mean track length (µm): 16.3

Track length reduction standard: 0.893

Etchant: 5.0M

Compositional parameter (µm): $D_{par}$

**2. Additional geological information**

| Assumption | Explanation and data source |
|---|---|
| Initial high temperature constraints at 400 ± 50 °C at apatite U-Pb age for each sample | Igneous samples. Apatite U-Pb ages from this study |
| Final constraint at surface conditions, 10 ± 10 °C at 0 Ma | Samples collected from surface |

**3. System and model specific parameters**
AHe radiation damage model: Flowers et al. (2009)
FT annealing model: Ketcham et al. (2007)
FT c-axis projection: no
Modelling code: QTQt 5.7.0 Windows
Iterations: Initial exploratory runs with 10,000 burn-in and 10,000 post burn-in. Final run 100,000 each burn-in and 100,000 post burn-in.
tT path characteristics: Reheating allowed
Acceptance rates: 0.2-0.8. Birth/death 1
Fitting criteria: Model specific observed vs. predicted values comparison below
Range of general prior: t=AFT central age ± AFT central age, T = 70 °C ± 70 °C.
*Data source*:
(1) - this study

## 4.1 Thermal history modelling output

Figure S15: Thermal history modelling outputs from QTQt, showing the observed and predicted values for the inputs. Note: slight differences may exist between the values here and elsewhere in the paper as a result of the internal calculations performed by QTQt.

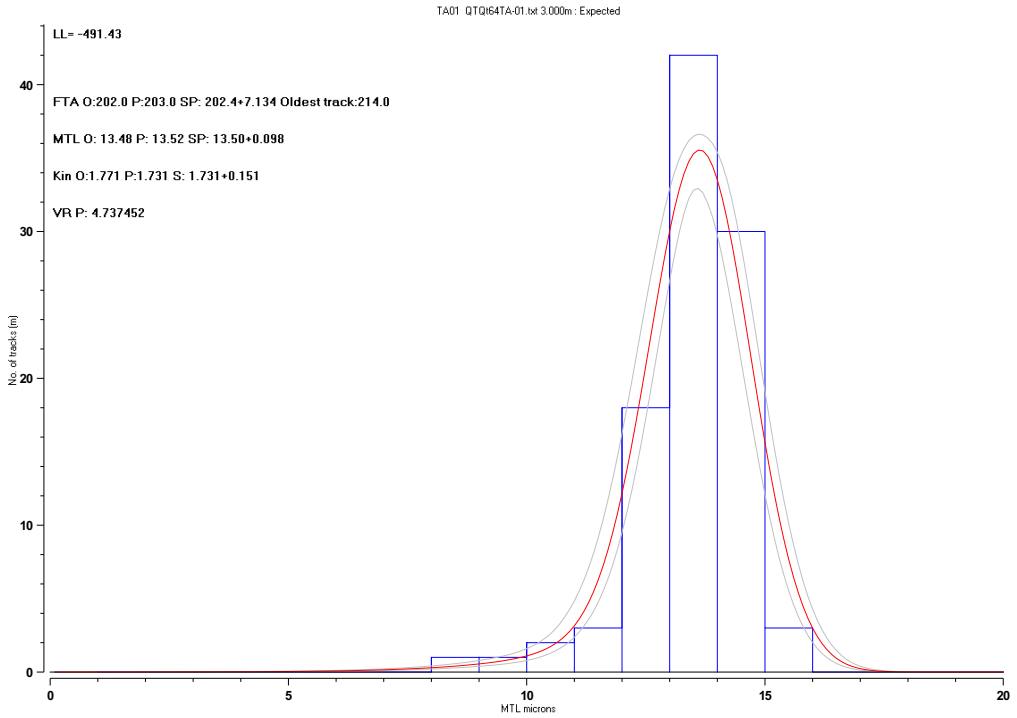


(a) Thermal history modelling output for TA01

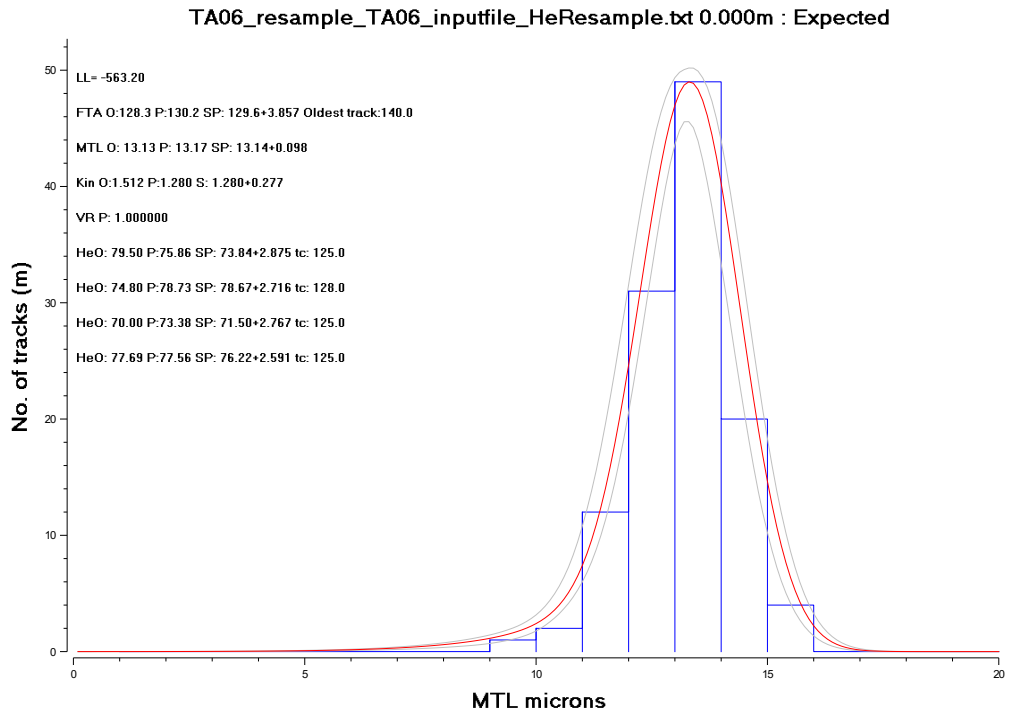


(b) Thermal history modelling output for TA06

Figure S16: Thermal history modelling outputs

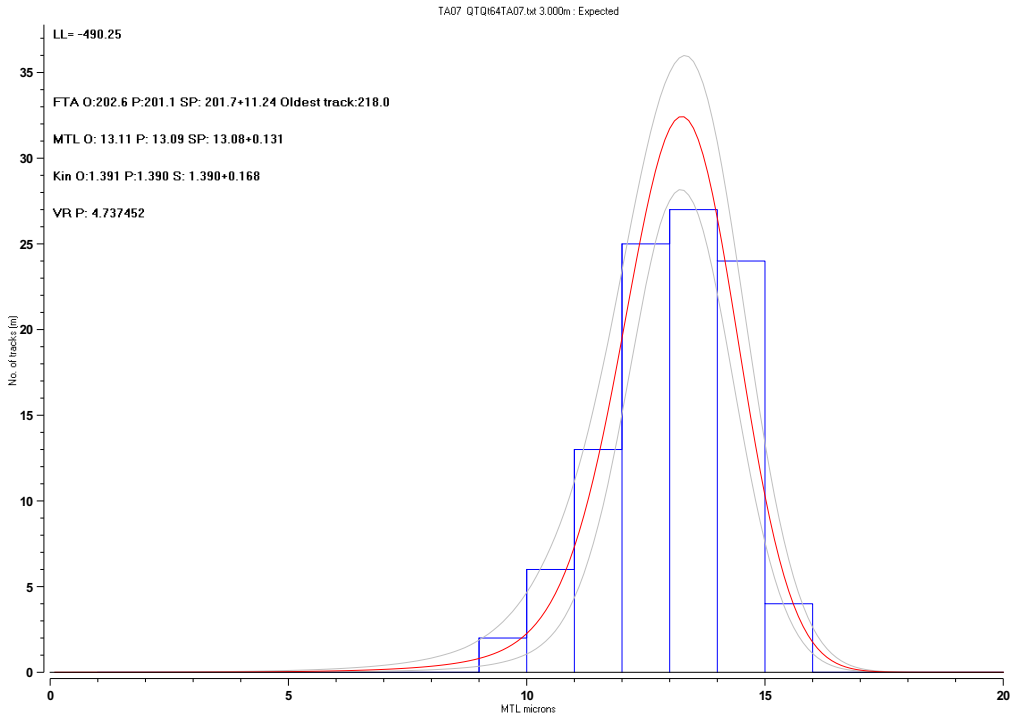


(a) Thermal history modelling output for TA07

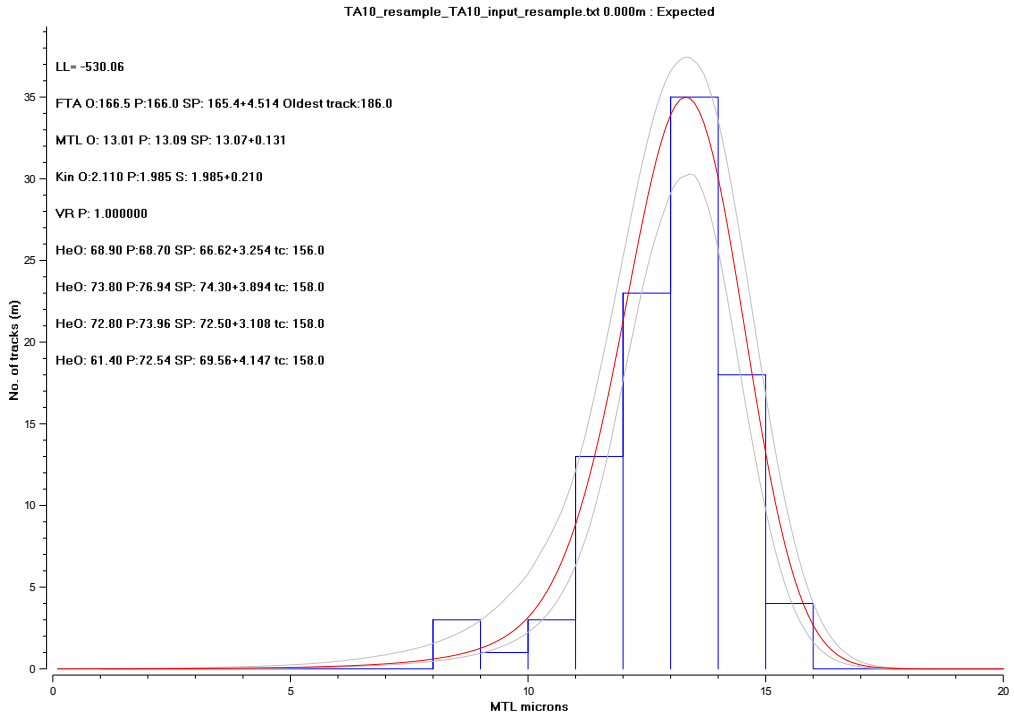


(b) Thermal history modelling output for TA10

Figure S17: Thermal history modelling outputs

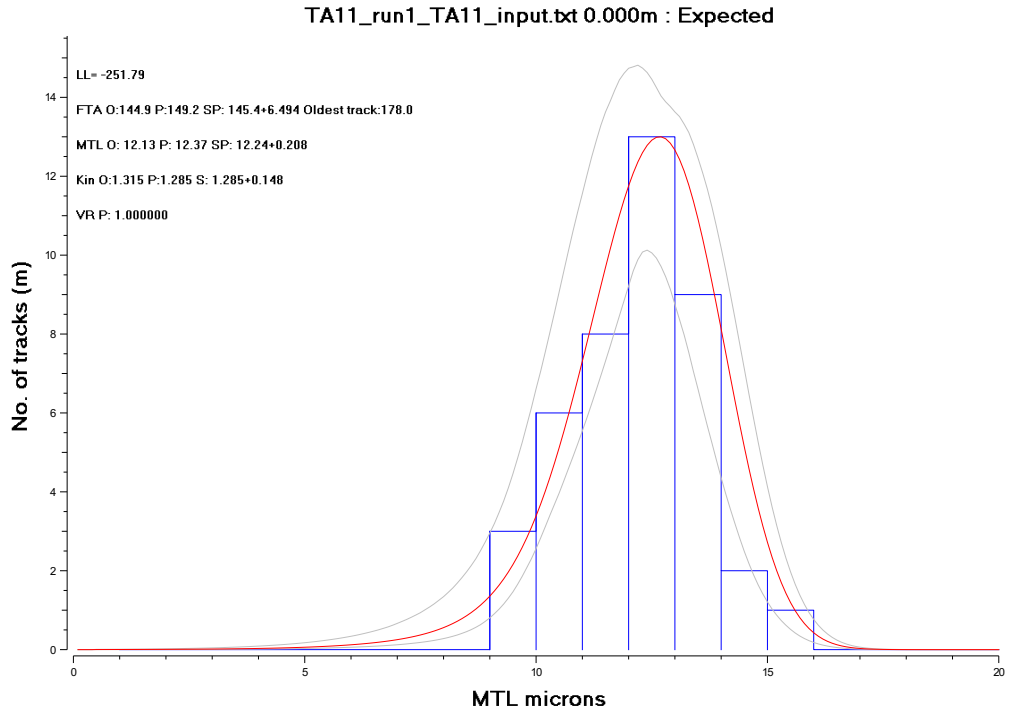


(a) Thermal history modelling output for TA11

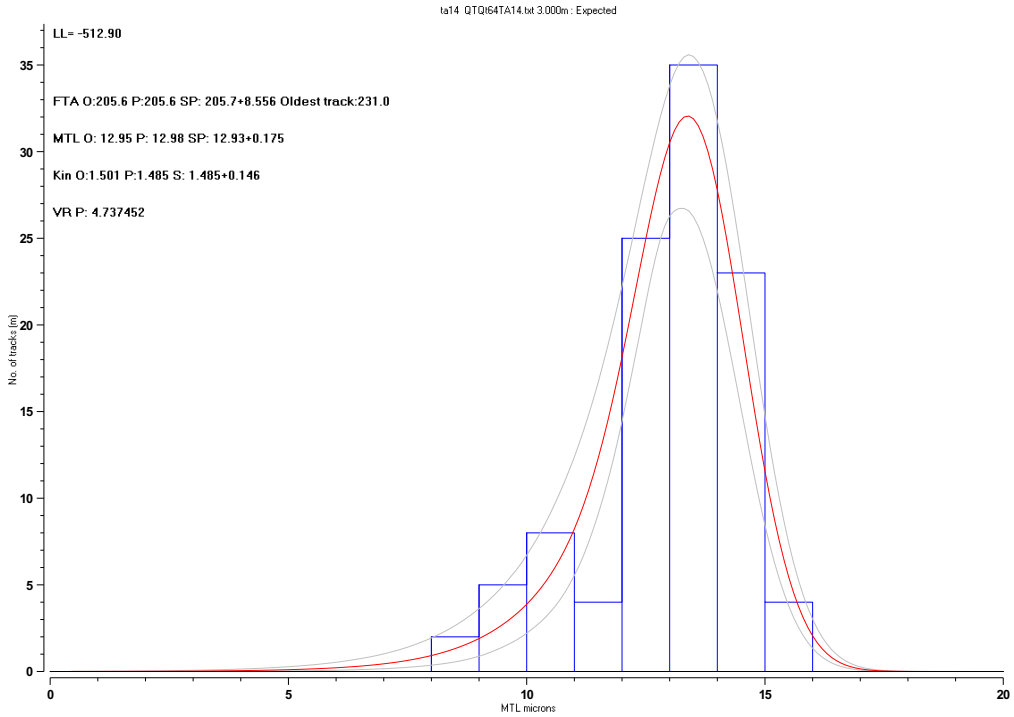


(b) Thermal history modelling output for TA14

Figure S18: Thermal history modelling outputs

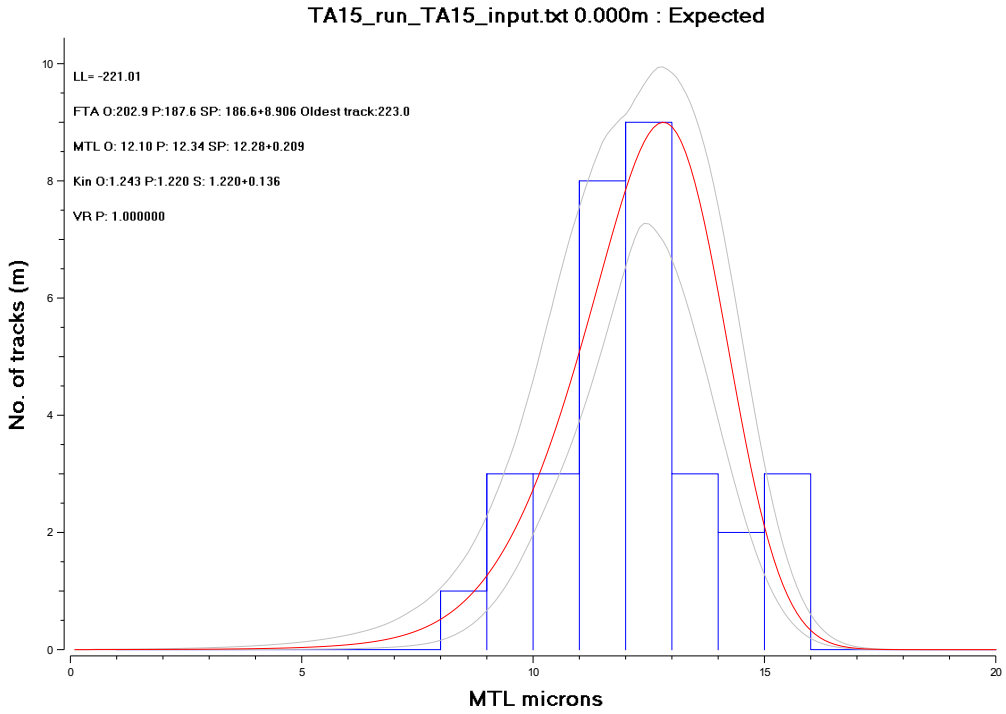


(a) Thermal history modelling output for TA15

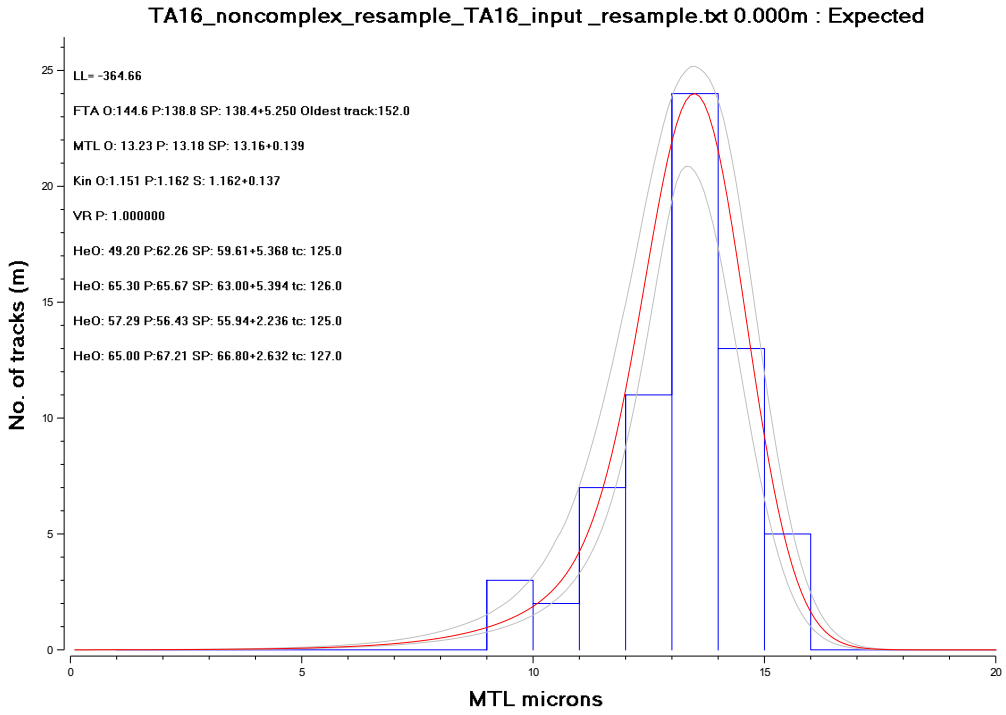


(b) Thermal history modelling output for TA16

Figure S19: Thermal history modelling outputs

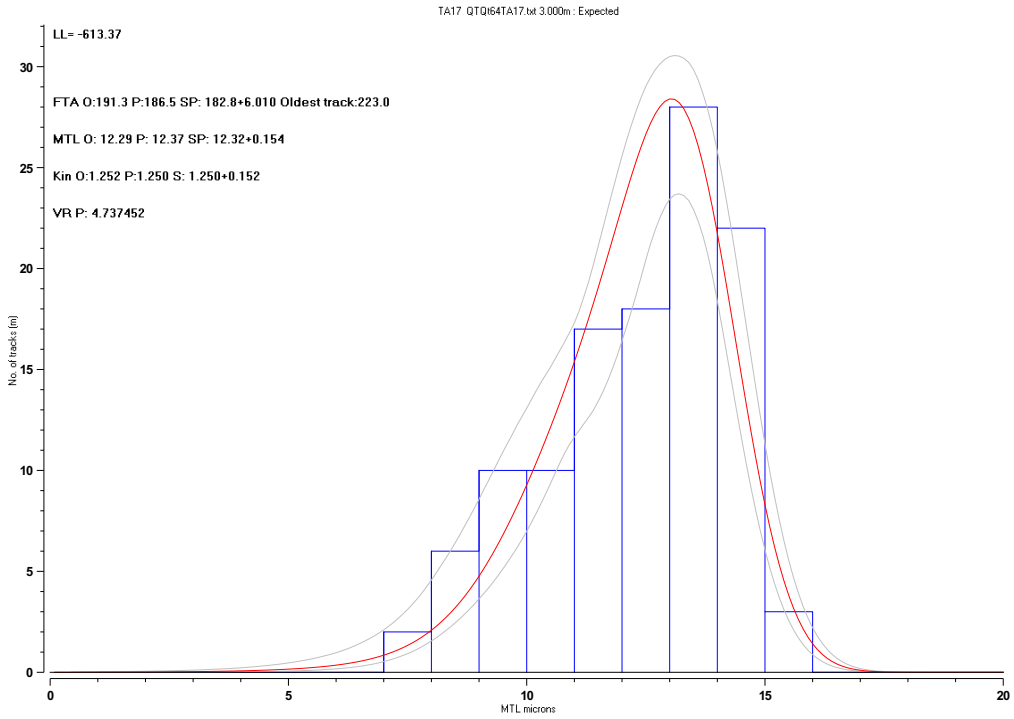


(a) Thermal history modelling output for TA17

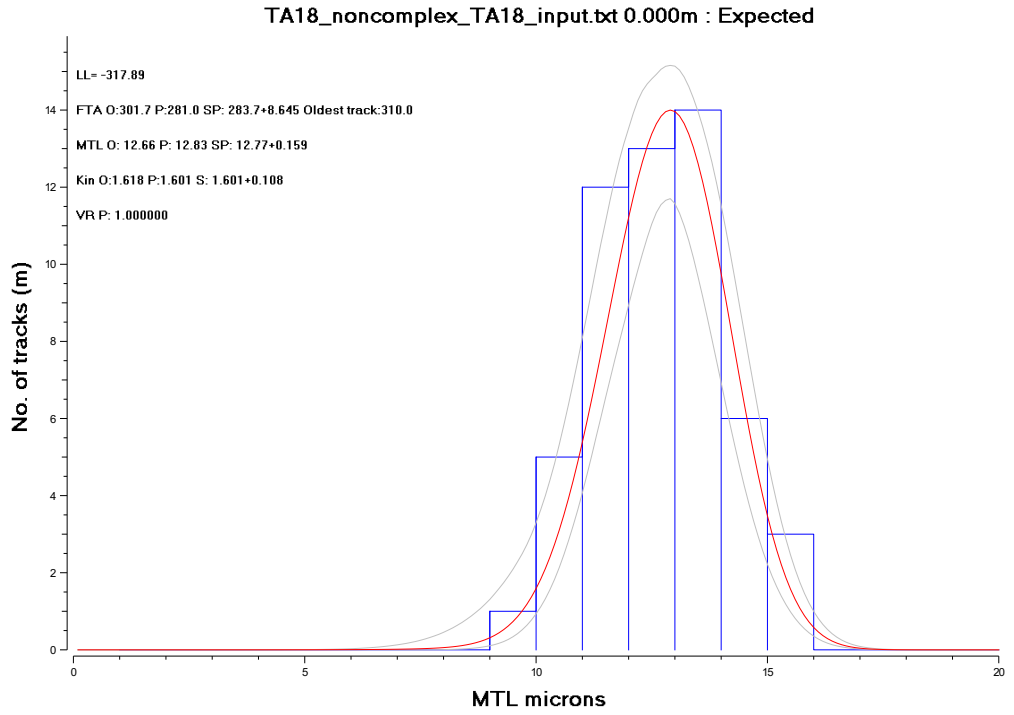


(b) Thermal history modelling output for TA18

Figure S20: Thermal history modelling outputs

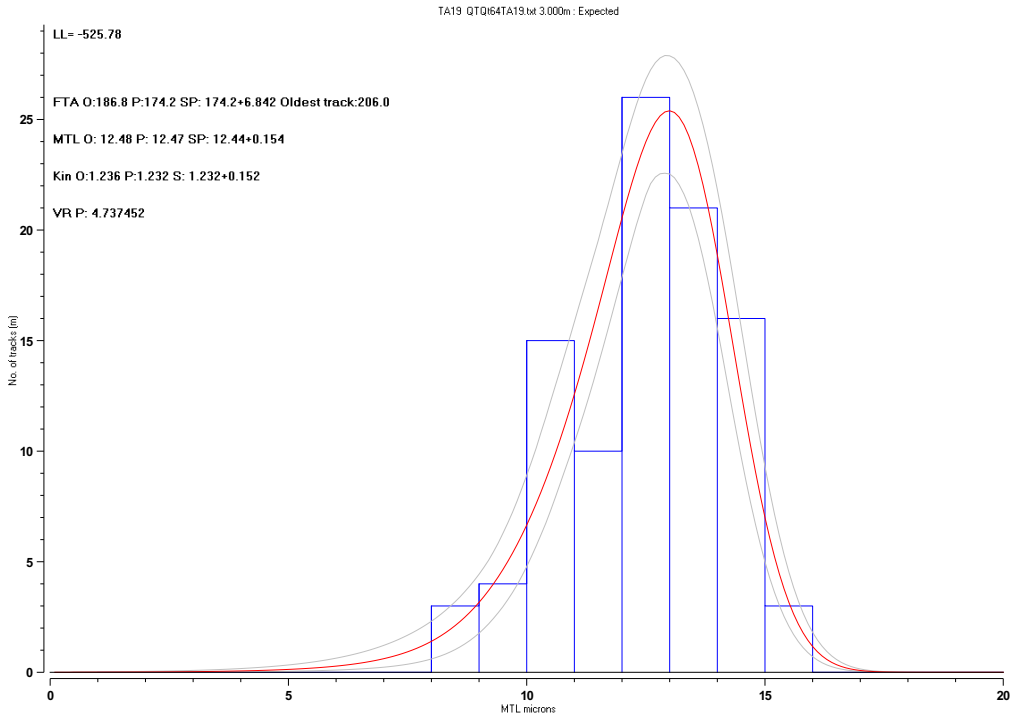


(a) Thermal history modelling output for TA19

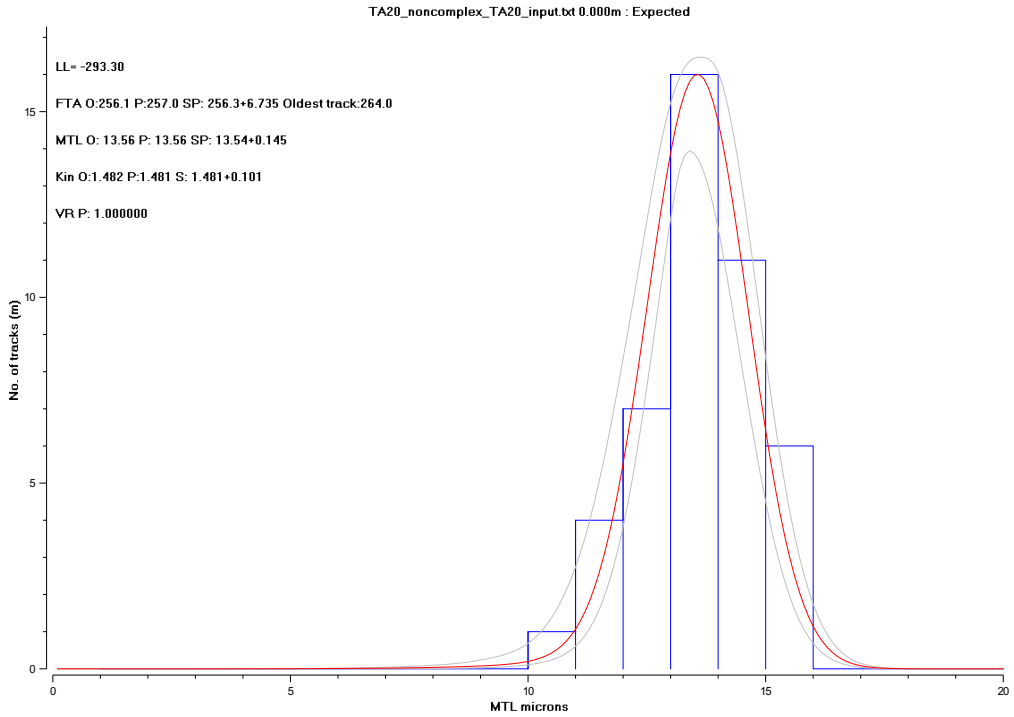


(b) Thermal history modelling output for TA20

Figure S21: Thermal history modelling outputs

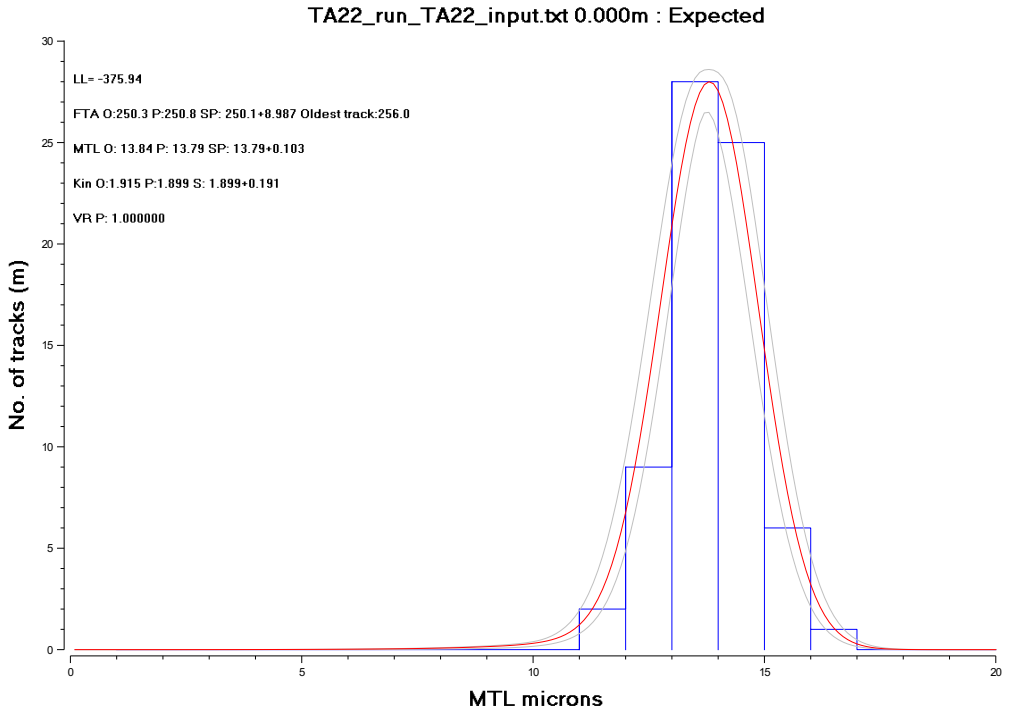


(a) Thermal history modelling output for TA22

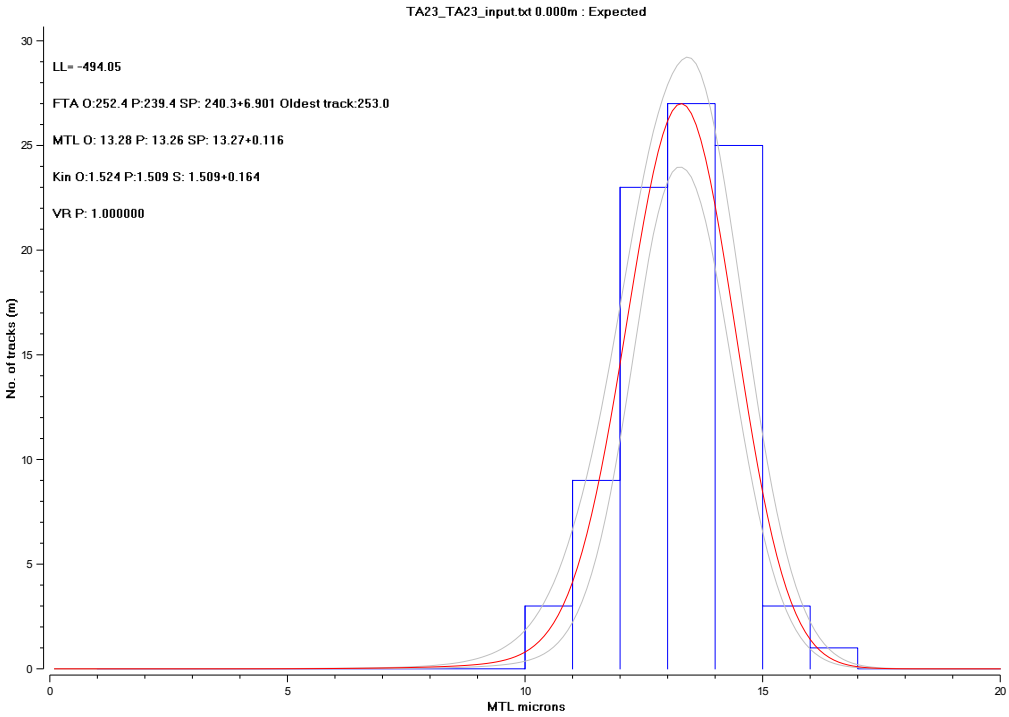


(b) Thermal history modelling output for TA23

Figure S22: Thermal history modelling outputs

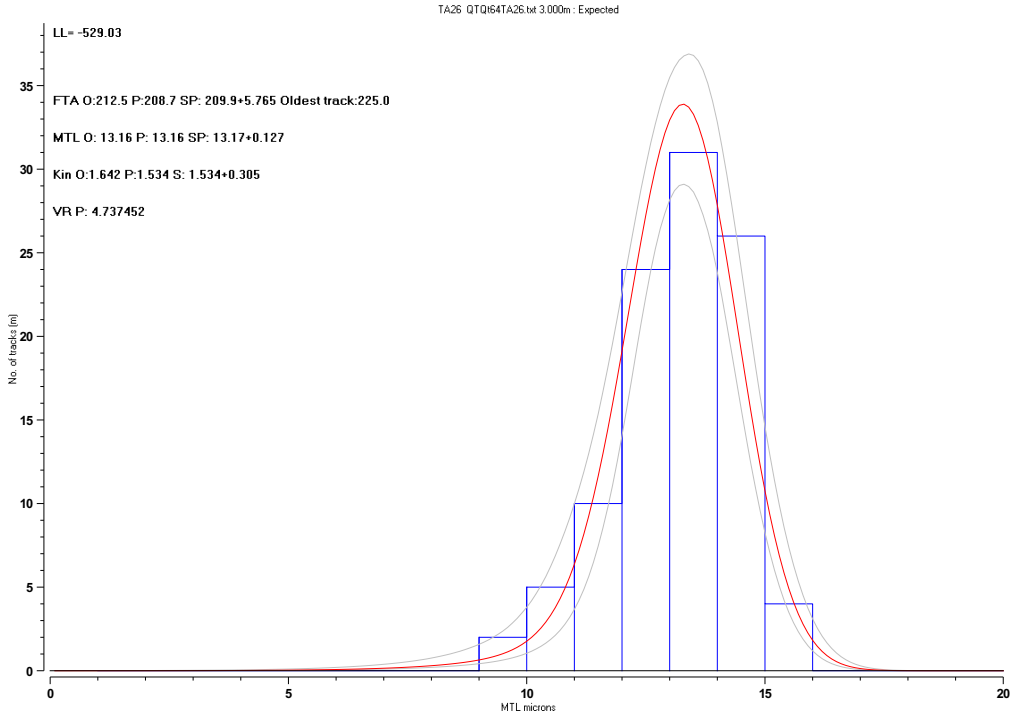


(a) Thermal history modelling output for TA26

# References

Farley, K. A., R. A. Wolf, and L. T. Silver (1996). "The effects of long alpha-stopping distances on (U-Th)/He ages". In: *Geochimica et Cosmochimica Acta* 60.21, pp. 4223–4229.

Flowers, R. M., R. A. Ketcham, D. L. Shuster, and K. A. Farley (2009). "Apatite (U–Th)/He thermochronometry using a radiation damage accumulation and annealing model". In: *Geochimica et Cosmochimica Acta* 73.8, pp. 2347–2365.

Ketcham, R. A., A. Carter, R. A. Donelick, J. Barbarand, and A. J. Hurford (2007). "Improved modeling of fission-track annealing in apatite". In: *American Mineralogist* 92.5-6, pp. 799–810.

Vermeesch, P. (2018). "IsoplotR: a free and open toolbox for geochronology". In: *Geoscience Frontiers* 9, pp. 1479–1493.